Islamic University Journal of Applied Sciences (IUJAS)

https://journals.iu.edu.sa/jesc

Volume VIII, Issue II, December 2026, Pages 326- 345

Variable Thermal Conductivity of Sutterby Nanofluid flow: a Numerical Study

Saima Riasat*, Saira Iqbal and Sadaf Riasat

Department of Mathematical Sciences Fatima Jinnah Women University, Rawalpindi, Pakistan

*Corresponding author: (Saima Riasat), Email Address: **saimaqau@live.com**

Abstract

The current research focuses on the impact of variable thermal conductivity on electro-magnetohydrodynamic (EMHD) flow of a Sutterby nanofluid in a Darcy-Forchheimer porous media with a stretching sheet. The impacts of thermal radiation and Christov-Cattaneo heat flux model are also considered in the study. The similarity approach is used to transform the governing mathematical model into a set of nonlinear ODEs which are then numerically solved by applying the BVP4C method. The detailed parametric studies are performed to provide more insights into the fluid flow and heat transfer behavior. It is found that the increase in magnetic field and velocity slip parameters decreases the fluid velocity. Also, the rise in the variable thermal conductivity parameter increases the temperature profile. The impacts of several controlling parameters on the velocity, temperature, concentration, skin friction coefficient, heat transfer rate, and Nusselt number are discussed and illustrated graphically and in tabular form.

Keywords: Electro-magnetohydrodynamic; Thermal radiation; Sutterby nanofluid; Darcy-Forchheimer porous media.

https://doi.org/10.63070/jesc.2026.045

Received 09 August 2026; Revised 02 October 2026; Accepted 10 October 2026. Available 16 October 2026.

Published by Islamic University of Madinah on behalf of *Islamic University Journal of Applied Sciences.*

This is an open access article published under the Creative Commons Attribution 4.0 International license (CC BY 4.0): https://creativecommons.org/licenses/by/4.0/

Nomenclature

c Positive constant $\left(s^{-1}\right)$

Q Heat source

B_0 Uniform magnetic field

Ha Magnetic parameter

Ec Eckert number

De Deborah number

Le Lewis number

F^* Inertia parameter

E Electric parameter

k_p Porosity parameter

Re Reynolds number

C^* Concentration

C_∞ Ambient concentration

C_W Concentration of the wall

Nt Thermophoretic parameter

Pr Prandtl number

Nb Brownian ratio parameter

R Radiation parameter

T_1 fluid temperature

T_∞ Ambient temperature

T_W wall temperature

k^* Mean absorption coefficient

D_T Thermophoretic diffusion co-efficient.

D_B Brownian diffusion co-efficient.

N_0 Slip length

K_0 Thermal jump length

C_b Drag coefficient

b^2 Consistency index

x, y Cartesian coordinates

U_W Stretching velocity

Greek letters

ε Thermal conductivity parameter

η Dimensionless similitude parameter

γ Thermal relaxation parameter

α Thermal diffusivity

λ^* Thermal relaxation time

σ Stefan Boltzmann constant

γ_1 Chemical reaction parameter

υ Fluid kinematic viscosity

ϕ Dimensionless concentration

ρ Fluid density

β Thermal slip parameter

σ^* Magnetic permeability

θ Dimensionless temperature

τ Nanoparticles to base fluid heat capacity ratio

δ Velocity slip parameter

Subscripts

f Fluid

∞ Ambient state

W On the sheet surface

1. Introduction

Nanofluids are the colloidal suspensions of base fluid with nanoparticles. Nanoparticles are the particles of dimensions approximately 1-100nm in size [1]. Nanofluids are fluids that are considered to enhance thermal conduction and heat convective transmission. Due to their significant applications in bubble absorption technologies [2], reactors [3], coolants [4], pharmaceutical procedure [5], heat exchangers [6], and solar collectors [7], nanofluids have attracted huge interest in recent years. Nanofluids are the term used by Choi et al. [8] to describe the dispersion of tiny nanoparticles within the base fluid. Bachok et al. [9] analyzed two-dimensional nanofluid flow on top of an expanding sheet. The water-based nanofluids flow along a stretched surface signified by a magnetic field was analyzed by Ali et al. [10] and Hamad [11]. Ibrahim et al. [12] analyzed MHD stagnation point nanofluid flow across a stretching surface.

Non-Newtonian fluids have recently piqued the interest of many analysts in the logical and design fields, as they have significant role in industrial and engineering mechanism. The Sutterby fluid [13] is a non-Newtonian fluid, and Sutterby published the basic equations for it in 1966. Due to its dual nature, that describes the behavior of both pseudo-plastic and dilatant fluid, the Sutterby fluid model has attracted the attention of researchers. These fluids include methylcellulose, hydroxyethyl cellulose, and carboxy-methylcellulose. A numeric investigation using Sutterby fluid theory with helical flow was presented by Eissa and Batra [14]. The mixed radiative and convective flow for squeezed Sutterby fluid through a squeezed channel was analyzed by Ahmad et al. [15]. The magnetic field influence of the Sutterby fluid combined with a mass and heat transition was described by Bilal et al. [16]. The Sutterby fluid was discussed in terms of entropy formation by Hayat et al. [17]. The impact of a linearly stretchy surface on the Sutterby nano-liquids flow is examined by Mir et al. in their study from [18]. On a stretching sheet, Bilal et al. [19] investigate a radiative Sutterby fluid with slip boundary conditions.

Because of the numerous uses in industry and engineering, many experts have long been immersed in evaluating fluid flow across porous space. Darcy's theory is commonly used to simulate and evaluate any flow across a permeable medium. The fluid flow in a porous material turns non-linear at higher velocities, and so the inertia impacts may not be neglected. Whereas conventional Darcy's theory is adequate for lower porosity and velocity, it is inadequate for inertial and boundary impacts at higher flow rates. Hence, Forchheimer [20] incorporated these concerns into the Darcian velocity equation by inserting an extra term using square velocity. This important development within law created a brand-new field for study with porous medium. Muskat [21] named the additive term within the Darcy law the Forchheimer term.

Khan et al. [22] analyzed the consequence of viscous dissipation and ohmic heating on ferrofluid Darcy-Forchheimer flow across a stretchable surface. Eid and Mabood [23] illustrated Darcy-Forchheimer motion on a dusty nanofluid over a expanding surface by using porosity media and magnetic field effect. Ramzan et al. [24] investigated the MHD Darcy Forchheimer flow of Williamson nanofluid along a stretching sheet.

Heat transfer is a natural phenomenon that occurs as a consequence of a temperature difference in the same bodies and among the different bodies. In the past centuries, Fourier's principle of heat conduction was used to examine the characteristics in heat transport. One of the model's major flaws are that it creates a parabolic heat equation, which causes a minor disruption to be sensed quickly across the whole substance. To overcome such barrier, Cattaneo [25] modified Fourier law by incorporating thermal relaxation time that permits heat to get transmitted by the slow propagation of thermal waves. The model was recognized as CC heat flux model. Straughan [26] investigate the Christov-Cattaneo model using thermal convection. Zampoli and Tibulle[27] investigated the incompressible fluid flow with Christov-Cattaneo heat flux model. Han et al. [28] used the Cattaneo model to examine the Maxwell boundary layer fluid flow. Hayat et al. [29] studied the effectiveness of Cattaneo model in flow across a expanding surface using varying thickness.

The amount of heat transfer from any material is referred as thermal conductivity. Another important attribute of thermal conductivity is that it varies with temperature. It is utilized in a variety of applications, including steam generators, laminating, concrete heating, electrolytes, moulding blow, and catalysis. Chiam [30-31] analyze the variable thermal conductivity effect on energy transmission. Gbadeyan et al. [32] investigated the 2D Casson nanofluid variable thermal conductivity and diffusivity moving across a stretchable sheet. Hamid et al. [33] employed the Galerkin technique to acquire the mathematical approximation for a nanofluid using variable thermal conductivity passing along a expanding sheet. Salawu and Dada [34] examine the impact of a magnetic field using varying thermal conductivity on an incompressible fluid passing through an expanding sheet. Abel et al. [35] analyze the thermal radiation effect on fluctuating thermal conductivity and temperature dependent thermal source.

Electro-magnetohydrodynamics is the dynamic description of the interaction of electrically conducting fluids with the influence of magnetic and electric fields. Having its various uses in magnetic drug targeting, biomedical engineering, engineering, and geophysics and in many other areas, EMHD has gained considerable attention over the years. The idea of flow control with EMHD was firstly used by Resler and

Sears [36]. In micro-channel flow regulation Chakraborty and Paul [37] established a mathematical model to investigate the EMHD effect. Buren et al. [38] investigate the flow of EMHD Newtonian fluid with corrugated walls in a tiny parallel channel. The Shah et al. [39] explore the CNTs rotating EMHD flow using thermal radiation effect passing through a stretching surface.

The goal of the present study is to examine the effect of variable thermal conductivity on the flow of EMHD Sutterby nanofluid passing through a stretching sheet. The numerical solutions is obtained using bvp4c approach built in MATLAB. The bvp4c method simply imposed the 3-stage Lobatto IIIa formula using a system of finite differences. This formulation used a collocation method having fourth-order accuracy and was widely accepted due to its strong stability properties [40-41]. The effect of various variables on velocity, temperature, and concentration profiles is depicted by employing graphs and tables. At last current findings are then compared to earlier research.

2. Problem Formulation

With the presence of Lorentz force the current study examines the 2-Dimensional EMHD (Electromagnetohydrodynamic) Sutterby nanofluid flow of Darcy-Forchheimer along a stretching sheet and the force is given as:

$$\vec{F} = \sigma^{*}\left(\vec{E} + \left(\vec{J} \times \vec{B}\right)\right). \tag{1}$$

The flow is on a sheet with stretching velocity $U_W = cx$. T_W is temperature constant that is expected on sheet surface. In the vertical axis, a constant magnetic field is considered (see Fig. 1).

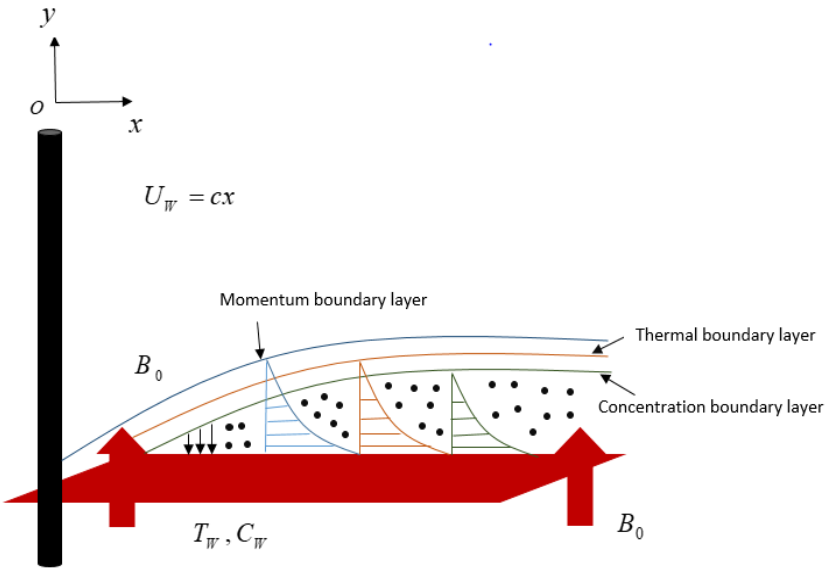


Fig. 1. Flow chart

By using above assumptions, the equations are:

$$\frac{\partial u_1}{\partial x}+\frac{\partial v_1}{\partial y}=0. \tag{2}$$

$$u_1\frac{\partial u_1}{\partial x}+v_1\frac{\partial u_1}{\partial y}=\frac{B_0\sigma^*}{\rho}\left(E_0-B_0u_1\right)+\frac{\upsilon}{2}\frac{\partial^2 u_1}{\partial y^2}\left(1-\frac{M_1b^2}{2}\left(\frac{\partial u_1}{\partial y}\right)^2\right)-Fu_1{}^2-\frac{\upsilon}{\kappa^*}u_1. \tag{3}$$

$$u_1\frac{\partial T_1}{\partial x}+v_1\frac{\partial T_1}{\partial y}=\frac{\mu}{\rho c_p}\left(\frac{\partial u_1}{\partial y}\right)^2+\frac{\partial}{\partial y}\left(\alpha\frac{\partial T_1}{\partial y}\right)+\frac{16\sigma T_\infty{}^3}{3k^*(\rho c)_f}\frac{\partial^2 T_1}{\partial y^2}+\frac{Q_O}{(\rho c_p)}\left(T_1-T_\infty\right) \tag{4}$$

$$+\tau\left[\frac{D_T}{T_\infty}\left(\frac{\partial T_1}{\partial y}\right)^2+D_B\frac{\partial T_1}{\partial y}\frac{\partial C}{\partial y}\right]+\frac{\sigma^*}{\rho c_p}\left(u_1B_0-E_0\right)^2-\lambda^*A*,$$

$$A*=u_1{}^2\frac{\partial^2 T_1}{\partial x^2}+\frac{\partial T_1}{\partial x}\left(u_1\frac{\partial u_1}{\partial x}+v_1\frac{\partial u_1}{\partial y}\right)+\frac{\partial T_1}{\partial y}\left(u_1\frac{\partial v_1}{\partial x}+v_1\frac{\partial v_1}{\partial y}\right)+v_1{}^2\frac{\partial^2 T_1}{\partial y^2}+2u_1v_1\frac{\partial^2 T_1}{\partial x\partial y}. \tag{5}$$

$$u_1\frac{\partial C^*}{\partial x}+v_1\frac{\partial C^*}{\partial y}+k_r\left(C^*-C_\infty\right)=D_B\frac{\partial^2 C^*}{\partial y^2}+\left(\frac{D_T}{T_\infty}\right)\frac{\partial^2 T_1}{\partial y^2}. \tag{6}$$

Here the components of velocity are u_1 and v_1. M_1 represents the deportment index of flow, consistency index is b^2, $F=C_b/x\sqrt{k^*}$ denotes inertia parameter, k^* represents mean absorption coefficient, k_r denotes chemical reaction parameter, E_0 represents the electric field strength, κ^* is the permeability of

porosity medium, D_T and D_B are the co-efficient of thermophoretic and Brownian diffusion, C_b denotes the drag parameter, $\alpha = \alpha_\infty \left[1 + \varepsilon\theta(\eta)\right]$ represents the variable thermal conductivity, ρ denotes the fluid density, Q_0 denotes heat source, λ^* is the thermal relaxation time and T_1 represents the fluid temperature.

The boundary constraints are:

$$U_W + N_0 \frac{\partial u_1}{\partial y} = u_1,\ T_1 = T_W + K_0 \frac{\partial T_1}{\partial y},\ v_1 = 0,\ C^* = C_W \text{ at } y = 0, \tag{7}$$

$$u_1 \to 0,\ T_1 \to T_\infty, C^* \to C_\infty \text{ at } y \to \infty.$$

Where the velocity of stretching sheet is $U_W = cx$, T_W denotes the wall temperature, N_0 is the slip length and $N_0 = K_0 = 0$ is observed for no-slip flow.

Using Similarity transformation:

$$u_1 = cxf'(\eta),\ v_1 = -\sqrt{c\upsilon} f(\eta),\ \theta(\eta) = \frac{T_1 - T_\infty}{T_W - T_\infty},\ \phi(\eta) = \frac{C^* - C_\infty}{C_W - C_\infty},\ \eta = \sqrt{\frac{c}{\upsilon}} y. \tag{8}$$

The transformed form of equations are:

$$f''' + 2Ha^2 (E - f') - \frac{M_1}{2} \mathrm{Re}\, Def'''(f'')^2 - 2k_p f' - 2(f')^2 - 2F^*(f')^2 + 2ff'' = 0, \tag{9}$$

$$\frac{1}{\mathrm{Pr}}\left(1 + \frac{4}{3}R + \varepsilon\theta\right)\theta'' + EcHa^2 (f' - E)^2 + \frac{\varepsilon\theta'^2}{\mathrm{Pr}} + Nt\theta'^2 + Q\theta + Ec(f'')^2 \tag{10}$$

$$+ Nb\theta'\phi' + f\theta' - \gamma\left(ff'\theta' + f^2\theta''\right) + EcHa^2 (f' - E)^2 = 0,$$

$$\phi'' + \frac{Nt}{Nb}\theta'' + \mathrm{Pr}\, Le\left[f\phi' - \gamma_1\phi\right] = 0. \tag{11}$$

The transformed boundary constraints are given as::

$$f(\eta) = 0,\ \theta(\eta) = 1 + \beta\theta',\ 1 + \delta f'' = f'(\eta),\ \phi(\eta) = 1 \text{ at } \eta = 0, \tag{12}$$

$$f' \to 0,\ \phi \to 0,\ \theta \to 0 \text{ at } \eta \to \infty.$$

The dimensionless variables occurring in equations

$$\Pr=\frac{\mu c_f}{k},\ Q=\frac{Q_0}{c\left(\rho c_p\right)},\ R=\frac{4\sigma T_\infty^3}{k^* k},\ Nt=\frac{\tau D_T\left(T_W-T_\infty\right)}{\upsilon T_\infty},\ Nb=\frac{\tau D_B\left(C_W-C_\infty\right)}{\upsilon},\tag{13}$$

$$Nt=\frac{\tau D_T\left(T_W-T_\infty\right)}{\upsilon T_\infty},\ \gamma=\lambda^* c,\ De=b^2c^2,\ Le=\frac{\alpha}{D_B},\ Ha=\sqrt{\frac{\sigma^*}{\rho c}}B_0,\ k_p=\frac{\upsilon}{\kappa^* c},\ \gamma_1=\frac{k_r}{c},$$

$$F^*=\frac{C_b}{\sqrt{k^*}},\ E=\frac{E_0}{xB_0c},\ \mathrm{Re}=\frac{cx^2}{\upsilon},\ Ec=\frac{c^2x^2}{c_p\left(T_W-T_\infty\right)}.$$

Skin shear stress, mass and heat transfer rate having mass flux j_m, shear stress τ_w and heat flux q_w are:

$$C_f=\frac{\tau_w}{\rho U_w^2},\ Sh_x=\frac{xj_m}{D_B\left(C_w-C_\infty\right)},\ Nu=\frac{xq_w}{k\left(T_w-T_\infty\right)},\tag{14}$$

$$q_w=-\left[\left(k+\frac{16\sigma T_\infty^3}{3k^*}\right)\frac{\partial T_1}{\partial y}\right],\ \tau_w=-\mu\left[\frac{\partial u_1}{\partial y}+\frac{M_1b^2}{3}\left(\frac{\partial u_1}{\partial y}\right)^3\right],\ j_m=-D_B\left(\frac{\partial C^*}{\partial y}\right).$$

Equation (8) and (14), gives

$$\mathrm{Re}_x^{1/2}\,C_{f_x}=-\left(f''(0)+(M_1/3)\,\mathrm{Re}\,De\left(f''(0)\right)^3\right),\tag{15}$$

$$Nu_x\,\mathrm{Re}_x^{-1/2}=-\left(1+\varepsilon\theta(0)+(4/3)R\right)\theta'(0),$$

$$Sh_x\,\mathrm{Re}_x^{-1/2}=-\phi'(0).$$

3. Numerical method of solution

The computational findings of the problem are obtained by employing bvp4c technique in MATLAB coding and problem is converted into first order by defining the new variables.

$$f=y_1,f'=y_2,f''=y_3,f'''=yy_1,\tag{16}$$

$$\theta=y_4,\theta'=y_5,\theta''=yy_2,\tag{17}$$

$$\phi=y_6,\phi'=y_7,\phi''=yy_3.\tag{18}$$

The transformed form of ordinary differential equation is obtained by using equations (16-18) into equations (9-11)

$$yy_1 = \frac{1}{1-\frac{M_1}{2}\mathrm{Re}\,Dey_3^{\,2}}\left(2y_2^{\,2} - 2Ha^2\left(E - y_2\right) - 2y_1y_3 + 2F^*y_2^{\,2} + 2k_p y_2\right), \tag{19}$$

$$yy_2 = \frac{1}{1+\varepsilon y_4 + \frac{4}{3}R}\left(-\varepsilon y_5^{\,2} - EcHa^2\left(y_2 - E_1\right)^2 + \mathrm{Pr}\left(-y_1y_5 + \gamma\left(y_1y_2y_5\right) - Nty_5^{\,2} - Ecy_3^{\,2} - Nby_5y_7 - Qy_4\right)\right), \tag{20}$$

$$yy_3 = -\frac{Nt}{Nb}yy_2 - \mathrm{Pr}.Le\left(y_1y_7 - \gamma_1y_6\right). \tag{21}$$

Transformed boundary constraints are:

$$y_1(\eta) = 0,\ y_4(\eta) = 1 + \beta y_5(\eta),\ y_2(\eta) = 1 + \delta y_3(\eta),\ y_6(\eta) = 1 \text{ at } \eta \to 0, \tag{22}$$

$$y_2(\eta) = 0,\ y_5(\eta) = 0,\ y_7(\eta) = 0 \text{ at } \eta \to \infty.$$

4. Results and discussion

This segment depicts the various physical variables impact on various profiles.

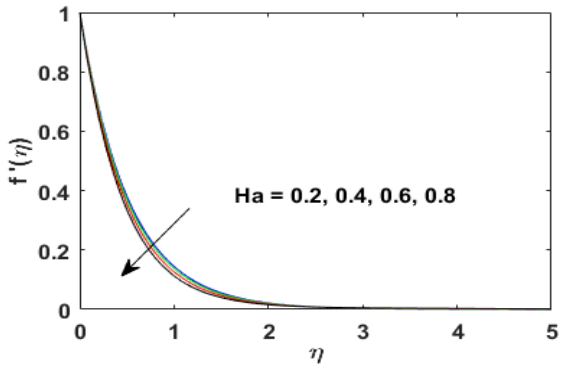


Fig. 2a: Velocity profile $f'(\eta)$ for varying Ha

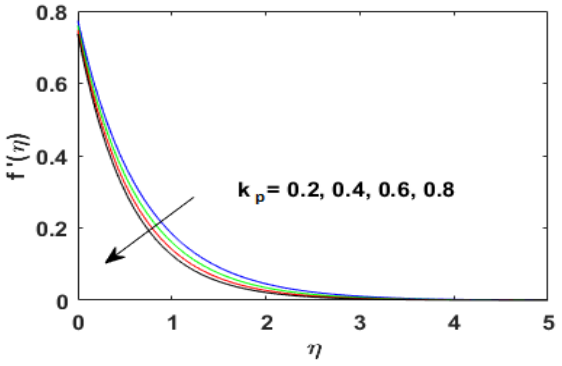


Fig. 2b: Velocity profile $f'(\eta)$ for varying k_p

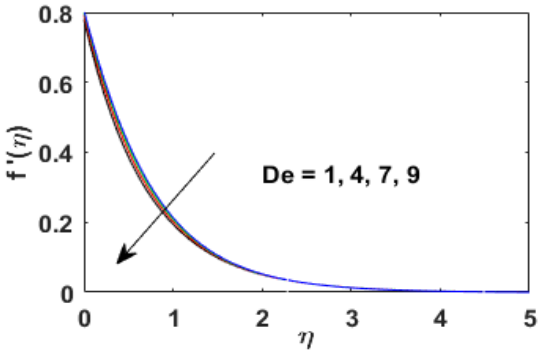


Fig. 3a: Velocity profile $f'(\eta)$ for varying De

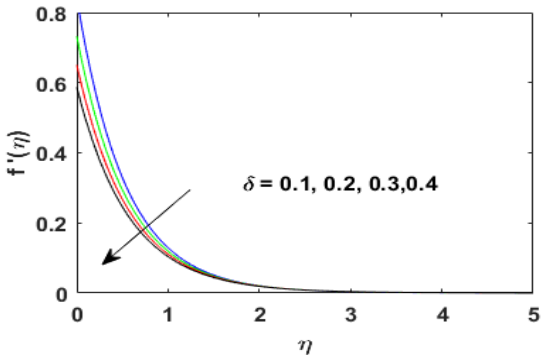


Fig. 3b: Velocity profile $f'(\eta)$ for varying δ

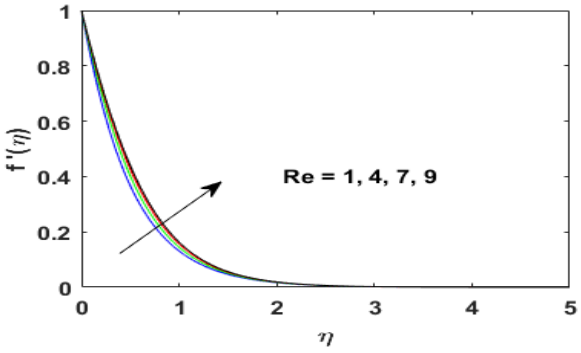


Fig. 4: Velocity profile $f'(\eta)$ for varying Re

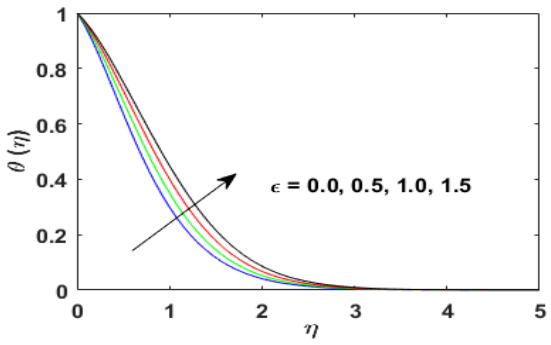


Fig. 5a: Velocity profile $f'(\eta)$ for varying ε

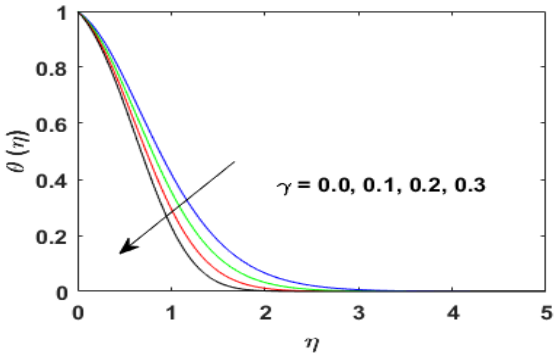


Fig. 5b: Velocity profile $f'(\eta)$ for varying γ

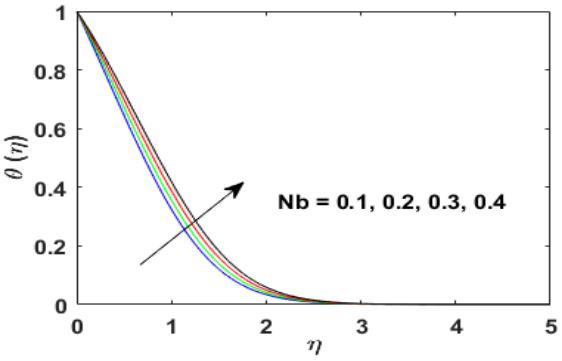


Fig. 6a: Temperature profile $\theta(\eta)$ for varying *Nb*

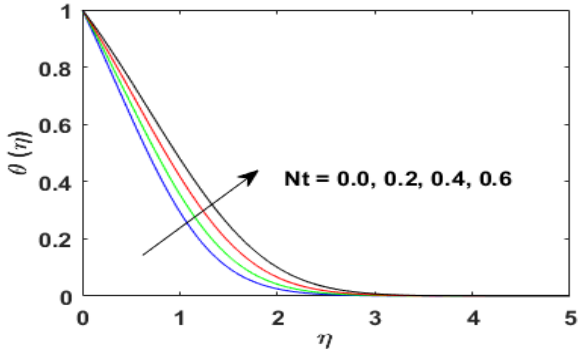


Fig. 6b: Temperature profile $\theta(\eta)$ for varying *Nt*

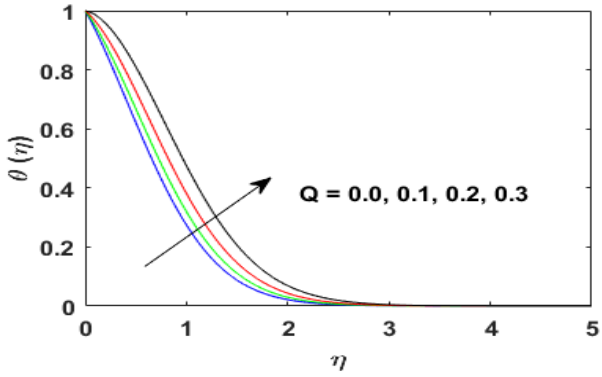
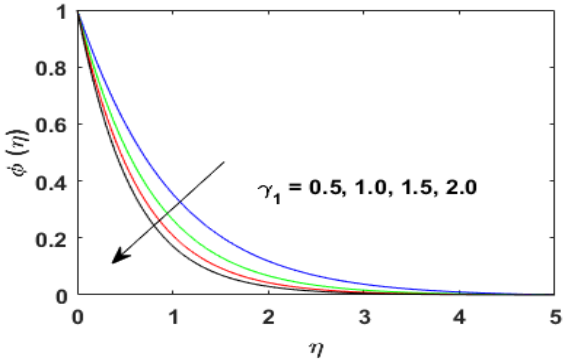


Fig. 7: Temperature profile $\theta(\eta)$ for varying Q



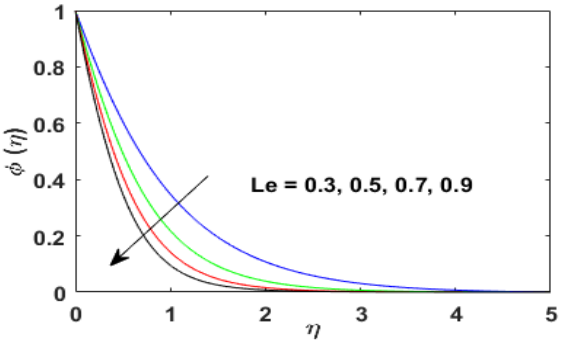


Fig. 8a: Concentration profile $\phi(\eta)$ for varying γ_1

Fig. 8b: Concentration profile $\phi(\eta)$ for varying for Le

Fig 2a. and Fig 2b depict the effect of both the magnetic field parameter Ha and porosity parameter k_p on $f'(\eta)$. It is observed that as the magnetic field variable increases, velocity profile shows decreasing trend (see Fig. 2a). The reason is that the Lorentz force rises physically when Ha increases. Hence increased in resistance to fluid motion that decrease the velocity of fluid. Furthermore, $f'(\eta)$ decelerates as value of k_p is increased (see Fig. 2b). The reason is that porosity parameter is inversely proportion to porous medium permeability. Thus, the lager value of k_p gives greater resistance. The influence of De and velocity slip parameter δ on the $f'(\eta)$ is depicted in Fig.3a and Fig. 3b. The Deborah number measures the material's viscoelastic properties. The larger value of De, means solid substance, the lower value of De means fluid substances. In the figure it is seen that by accelerating the values of De velocity profile decreases (see Fig. 3a). Similarly, velocity profile decreases when the slip factor increases (see Fig. 3b). The reason is that the velocity of fluid along the stretching sheet are not same with the stretching velocity of sheet due to the slip phenomenon. The impact of Reynolds number Re on $f'(\eta)$ is depicted in Fig. 4. The velocity profile rises as the Reynolds number accelerates. This is due to fact that the Reynold number describes the relationship of inertial and viscous forces, hence the larger value of Reynold number accelerates the velocity profile because of dominance of inertial forces.

In Fig. 5a and Fig. 5b the coefficient of variable thermal conductivity ε and the thermal relaxation γ impact on $\theta(\eta)$ is depicted. In Fig. 5a it is observed that $\theta(\eta)$ rises by increasing the value of the variable thermal conductivity parameter. Increased thermal conductivity implies greater kinetic energy among molecules, leading to a higher number of molecular interactions and, as a result, a direct link among temperature and kinetic energy. Conversely, as the inputs of γ accelerates $\theta(\eta)$ decelerates. This is due to raising thermal relaxation parameter allows material particles to take larger time to exchange heat with nearby particles (see Fig. 5b). In Fig. 6a and Fig. 6b it is noticed that the fluid temperature accelerates as inputs of the Nb and Nt enhances. The reason is that the by enhancing the Brownian motion parameter intensifies the nanofluid thermal conductivity hence temperature profiles increase (see Fig. 6a). In the same way as the value of Nt increases, the thermophoresis force accelerates, leading the nanoparticles to

migrate from hot to cold region hence the temperature profile to accelerate (see Fig. 6b). In Fig. 7 the temperature profile fluctuates as the value of heat source parameter Q accelerates. The reason is that when heat generation increases the fluids temperature rises.

In Fig. 8a and Fig. 8b. the impact of scaled chemical reaction parameter γ_1 and the Lewis number Le on the concentration profile is depicted. By changing the values of γ_1, decelerates the $\phi(\eta)$. This is due to fact that rising the impact of γ_1 accelerates the intermolecular mass transfer rate which causes the volumetric reduction in nanoparticles (see Fig. 8a). Moreover, as the Lewis number rises then concentration profile diminishes (see Fig. 8b). The fact is that the rate of mass transfer rises as the Lewis number accelerates.

Tables 1, 2 and 3 demonstrate the impact of different physical variables on Nusselt number, skin friction and mass transfer rate. In Table 1 it can be noticed that skin friction coefficient accelerates for k_p, Re and De, but reduces for M. In Table 2 it is noticed that heat transfer rate accelerates by accelerating the values of R but decelerate with Nb and Nt. In Table 3 it is discovered that $-\phi'(0)$ increases for Nt, Le but decreases for Nb.

Table 1: Impact of k_p, De, Re, M on $\mathrm{Re}_x^{\frac{1}{2}} C_f$.

De	Re	M	k_p	$\mathrm{Re}_x^{\frac{1}{2}} C_f$
-	-	-	0.1	0.7280
0.1	0.1	0.1	0.2	0.7401
-	-	-	0.3	0.7575
-	-	0.1	-	0.7382
0.1	0.1	0.2	0.1	0.7348
-	-	0.3	-	0.7296
-	2	-	-	0.7310
0.2	3	0.1	0.1	0.7490
-	4	-	-	0.8140
0.2	-	-	-	0.7480
0.4	3	0.1	0.1	0.7721
0.6	-	-	-	0.7939

Table 2: Impact of Nb, Nt and R on $Nu_x \operatorname{Re}_x^{-1/2}$

Nt	Nb	R	$Nu_x \operatorname{Re}_x^{-1/2}$
-	0.1	-	0.164715
0.2	0.2	0.2	0.163103
-	0.3	-	0.161498
-	-	0.1	0.170202
0.1	0.1	0.2	0.172369
-	-	0.4	0.175646
0.1	-	-	0.168343
0.2	0.2	0.1	0.166608
0.3	-	-	0.164880

Table 3: Impact of Nt, Le and Nb on $-\phi'(0)$

Nt	Le	Nb	$-\phi'(0)$
-	0.1	-	0.23388
0.1	0.2	0.1	0.244731
-	0.3	-	0.255486
-	-	0.1	0.260419
0.1	0.1	0.2	0.237574
-	-	0.3	0.229952
0.1	-	-	0.234226
0.2	0.2	0.2	0.248435
0.3	-	-	0.264422

5. Conclusions

In this study, the impact of variable thermal conductivity on two-dimensional EMHD flow of Sutterby nanofluid by considering Cattaneo Christov heat flux model in the presence of porous media over a stretching sheet was analyzed. The graphical outcomes are examined by varying the input variables. The findings are:

- The effect of Hartmann number Ha , velocity slip parameters δ, Deborah number De and Porosity parameter k_p decreases the velocity profile.
- The velocity distribution accelerates by increasing the Reynold number Re.
- The accelerating values of γ declines the temperature of fluid but the larger input of Q, Nt, Nb and ε increases the temperature.
- The concentration profile decelerates by using the larger inputs of Le and γ_1 .
- The skin shear stress accelerates by enhancing the values of k_p, Re and De but decelerates with accelerating values of M .
- The Nusselt number diminishes by rising the inputs of Nb and Nt but rises as radiation parameter increases.
- Sherwood number increases for Nt and Le, but decrease with increasing value of Nb .

6. Limitation and Future work

Present study has the following limitations

- ❖ Present study is two dimensional, with no slip boundary conditions.
- ❖ Other thermophysical quantities are not taken variable.
- ❖ Grid independent study is not carried out in the presence analysis.

The present study can be extended to:

- ❖ Carry out the sensitivity analysis.
- ❖ Convergence analysis to verify the authenticity of the numerical solution obtained.
- ❖ The electroosmotic flow can be considered as the electric and magnetic field are both applied.

Funding

The authors declare that this research received no external funding

Data Availability Statement

Data is given withing the manuscript.

Conflicts of Interest

The authors declare no conflict of interest.

References

[1] Sharma, G., Kumar, A., Sharma, S., Naushad, M., Dwivedi, R. P., ALOthman, Z. A., & Mola, G. T. (2019). Novel development of nanoparticles to bimetallic nanoparticles and their composites: a review. *Journal of King Saud University-Science*, *31*(2), 257-269.

[2] Su, F., Deng, Y., & Ma, H. (2015). Numerical analysis of ammonia bubble absorption in a binary nanofluid. *Chemical Engineering Communications*, *202*(4), 500-507.

[3] Zarifi, E., Jahanfarnia, G., & Veysi, F. (2013). Subchannel analysis of nanofluids application to VVER-1000 reactor. *Chemical Engineering Research and Design*, *91*(4), 625-632.

[4] Sreeremya, T. S., Krishnan, A., Mohamed, A. P., Hareesh, U. S., & Ghosh, S. (2014). Synthesis and characterization of cerium oxide based nanofluids: An efficient coolant in heat transport applications. *Chemical Engineering Journal*, *255*, 282-289.

[5] Tripathi, D., & Bég, O. A. (2014). Mathematical modelling of peristaltic pumping of nano-fluids. In *Modelling and Simulation of Diffusive Processes* (pp. 69-95). Springer, Cham.

[6] Ali, B., Hussain, S., Naqvi, S. I. R., Habib, D., & Abdal, S. (2021). Aligned magnetic and bioconvection effects on tangent hyperbolic nanofluid flow across faster/slower stretching wedge with activation energy: Finite element simulation. *International Journal of Applied and Computational Mathematics*, *7*(4), 1-20.

[7] Ali, B., Rasool, G., Hussain, S., Baleanu, D., & Bano, S. (2020). Finite element study of magnetohydrodynamics (MHD) and activation energy in Darcy–Forchheimer rotating flow of Casson Carreau nanofluid. *Processes*, *8*(9), 1185.

[8] Choi, S. U., & Eastman, J. A. (1995). *Enhancing thermal conductivity of fluids with nanoparticles* (No. ANL/MSD/CP-84938; CONF-951135-29). Argonne National Lab., IL (United States).

[9] Bachok, N., Ishak, A., & Pop, I. (2011). Stagnation-point flow over a stretching/shrinking sheet in a nanofluid. *Nanoscale research letters*, *6*(1), 1-10.

[10] Ali, B., Thumma, T., Habib, D., & Riaz, S. (2022). Finite element analysis on transient MHD 3D rotating flow of Maxwell and tangent hyperbolic nanofluid past a bidirectional stretching sheet with Cattaneo Christov heat flux model. *Thermal Science and Engineering Progress*, *28*, 101089.

[11] Hamad, M. A. A. (2011). Analytical solution of natural convection flow of a nanofluid over a linearly stretching sheet in the presence of magnetic field. *International communications in heat and mass transfer*, *38*(4), 487-492.

[12] Ibrahim, W., Shankar, B., & Nandeppanavar, M. M. (2013). MHD stagnation point flow and heat transfer due to nanofluid towards a stretching sheet. *International journal of heat and mass transfer*, *56*(1-2), 1-9.

[13] Sutterby, J. L. (1966). Laminar converging flow of dilute polymer solutions in conical sections: Part I. Viscosity data, new viscosity model, tube flow solution. *AIChE Journal*, *12*(1), 63-68.

[14] Batra, R. L., & Eissa, M. (1994). Helical flow of a Sutterby model fluid. *Polymer-Plastics Technology and Engineering*, *33*(4), 489-501.

[15] Ahmad, S., Farooq, M., Javed, M., & Anjum, A. (2018). Double stratification effects in chemically reactive squeezed Sutterby fluid flow with thermal radiation and mixed convection. *Results in physics*, *8*, 1250-1259.

[16] Bilal, S., Sohail, M., Naz, R., & Malik, M. Y. (2020). Dynamical and optimal procedure to analyze the exhibition of physical attributes imparted by Sutterby magneto-nanofluid in Darcy medium yielded by axially stretched cylinder. *Canadian Journal of Physics*, *98*(1), 1-10.

[17] Hayat, T., Bibi, F., Khan, A. A., & Alsaedi, A. (2021). Entropy production minimization and non-Darcy resistance within wavy motion of Sutterby liquid subject to variable physical characteristics. *Journal of Thermal Analysis and Calorimetry*, *143*(3), 2215-2225.

[18] Mir, N. A., Farooq, M., Rizwan, M., Ahmad, F., Ahmad, S., & Ahmad, B. (2020). Analysis of thermally stratified flow of Sutterby nanofluid with zero mass flux condition. *Journal of Materials Research and Technology*, *9*(2), 1631-1639.

[19] Bilal, S., Sohail, M., Naz, R., Malik, M. Y., & Alghamdi, M. (2019). Upshot of ohmically dissipated Darcy-Forchheimer slip flow of magnetohydrodynamic Sutterby fluid over radiating

linearly stretched surface in view of Cash and Carp method. *Applied Mathematics and Mechanics*, *40*(6), 861-876

[20] Forchheimer, P. (1901). Wasserbewegung durch boden. *Z. Ver. Deutsch, Ing.*, *45*, 1782-1788.

[21] Muskat, M. (1938). The flow of homogeneous fluids through porous media. *Soil Science*, *46*(2), 169.

[22] Khan, M. I., Alzahrani, F., & Hobiny, A. (2020). Simulation and modeling of second order velocity slip flow of micropolar ferrofluid with Darcy–Forchheimer porous medium. *Journal of Materials Research and Technology*, *9*(4), 7335-7340.

[23] Eid, M. R., & Mabood, F. (2021). Entropy analysis of a hydromagnetic micropolar dusty carbon NTs-kerosene nanofluid with heat generation: Darcy–Forchheimer scheme. *Journal of Thermal Analysis and Calorimetry*, *143*(3), 2419-2436.

[24] Ramzan, M., Gul, H., & Zahri, M. (2020). Darcy-Forchheimer 3D Williamson nanofluid flow with generalized Fourier and Fick's laws in a stratified medium. *Bulletin of the Polish Academy of Sciences. Technical Sciences*, *68*(2).

[25] Cattaneo, C. (1948). Sulla conduzione del calore. *Atti Sem. Mat. Fis. Univ. Modena*, *3*, 83-101.

[26] Straughan, B. (2010). Thermal convection with the Cattaneo–Christov model. *International Journal of Heat and Mass Transfer*, *53*(1-3), 95-98.

[27] Tibullo, V., & Zampoli, V. (2011). A uniqueness result for the Cattaneo–Christov heat conduction model applied to incompressible fluids. *Mechanics Research Communications*, *38*(1), 77-79.

[28] Han, S., Zheng, L., Li, C., & Zhang, X. (2014). Coupled flow and heat transfer in viscoelastic fluid with Cattaneo–Christov heat flux model. *Applied Mathematics Letters*, *38*, 87-93.

[29] Hayat, T., Farooq, M., Alsaedi, A., & Al-Solamy, F. (2015). Impact of Cattaneo-Christov heat flux in the flow over a stretching sheet with variable thickness. *Aip Advances*, *5*(8), 087159.

[30] Chiam, T. C. (1996). Heat transfer with variable conductivity in a stagnation-point flow towards a stretching sheet. *International Communications in Heat and Mass Transfer*, *23*(2), 239-248.

[31] Chiam, T. (1998). Heat transfer in a fluid with variable thermal conductivity over a linearly stretching sheet. *Acta mechanica*, *129*(1), 63-72.

[32] Gbadeyan, J. A., Titiloye, E. O., & Adeosun, A. T. (2020). Effect of variable thermal conductivity and viscosity on Casson nanofluid flow with convective heating and velocity slip. *Heliyon*, *6*(1), e03076.

[33] Hamid, M., Usman, M., Zubair, T., Haq, R. U., & Wang, W. (2018). Shape effects of MoS2 nanoparticles on rotating flow of nanofluid along a stretching surface with variable thermal conductivity: A Galerkin approach. *International Journal of Heat and Mass Transfer*, *124*, 706-714.

[34] Salawu, S. O., & Dada, M. S. (2016). Radiative heat transfer of variable viscosity and thermal conductivity effects on inclined magnetic field with dissipation in a non-Darcy medium. *Journal of the Nigerian Mathematical Society*, *35*(1), 93-106.

[35] Subhas, A., Prasad, K. V., & Mahaboob, A. (2005). Buoyancy force and thermal radiation effects in MHD boundary layer viscoelastic flow over continuously moving stretching surface. *Int. J. Therm. Sci*, *44*, 465-476.

[36] Resler Jr, E. L., & Sears, W. R. (1958). The prospects for magneto-aerodynamics. *Journal of the Aerospace Sciences*, *25*(4), 235-245.

[37] Chakraborty, S., & Paul, D. (2006). Microchannel flow control through a combined electromagnetohydrodynamic transport. *Journal of Physics D: Applied Physics*, *39*(24), 5364.

[38] Buren, M., Jian, Y., & Chang, L. (2014). Electromagnetohydrodynamic flow through a microparallel channel with corrugated walls. *Journal of Physics D: Applied Physics*, *47*(42), 425501.

[39] Shah, Z., Bonyah, E., Islam, S., & Gul, T. (2019). Impact of thermal radiation on electrical MHD rotating flow of Carbon nanotubes over a stretching sheet. *AIP Advances*, *9*(1), 015115.

[40] Laurent, O. J. (1996). Lobatto methods. *URL: https://homepage. math. uiowa. edu/~ ljay/publications. dir/Lobatto.*

[41] Ascher, U. M., Mattheij, R. M., & Russell, R. D. (1995). *Numerical solution of boundary value problems for ordinary differential equations*. Society for Industrial and Applied Mathematics.